

Effect of Flow Rate on the Corrosion Products Formed on Traditional and New Generation API 5L X-70 in a Sour Brine Environment

A. Cervantes Tobón^{1,*}, M. Díaz Cruz¹, M. A. Domínguez Aguilar², J. L. González Velázquez¹.

¹ Instituto Politécnico Nacional, Departamento de Ingeniería Metalúrgica, IPN-ESIQIE, U.P. Adolfo López Mateos, Zacatenco, C.P. 07738, México, D.F., México.

² Instituto Mexicano del Petróleo, Dirección de Investigación y Posgrado, Eje Central Norte Lázaro Cárdenas 152, Col. San Bartolo Atepehuacan, C.P. 07730, México D.F., México.

*E-mail: maenc_2000@yahoo.com.mx

Received: 27 November 2014 / Accepted: 3 February 2015 / Published: 24 February 2015

The effect of chemical composition on the nature of the corrosion products formed on pipe steels API 5L X-70 traditional and API 5L X-70 new generation was studied. General corrosion was induced under different flow rates (1~4 m/s) in a rotating disc electrode immersed in a sour brine solution with kerosene at 60 °C. Linear polarization resistance indicated that API 5L X-70 NG displayed a higher corrosion resistance because of the presence of copper, which promoted a greater amount of oxides than sulfides on surface in comparison to those formed in the traditional pipe steel. Moreover, ferrite increased (70-95%) and perlite decreased (30-5%) in NG steel to protect steel from further dissolution. Scanning electron microscopy of traditional steel displayed the presence of a larger amount of corrosion products with evident porosity and bush shape morphology, whereas corrosion products on NG pipe steel looked similar but more coherent and both covered most of the steel surfaces. X-ray diffraction analysis showed that the corrosion products are mainly composed of a mixture of oxides (maghemite, hematite, magnetite), and sulfides (mackinawite, troilite, pyrite, marcasite and smithite) only in the immersion tests. The protective function of corrosion products on the API 5L X-70 NG surface turned out to be better because of the presence of one different phase, triclinic pyrite, that seems more stable than cubic pyrite in traditional steel. The presence of copper in new generation steel in approximately twice as much compared to the traditional steel, which apparently favored the cathodic reaction where oxygen is formed. Chromium and nickel delayed anode reaction, ferrite dissolution, and helps to decrease corrosion rate.

Keywords: Corrosion, polarization resistance, pipeline steel, copper.

1. INTRODUCTION

Hydrogen sulfide (H_2S) present in the oil transport pipelines is one of the main agents of corrosion. In this process atomic hydrogen H^+ is formed on pipeline surface; which is adsorbed and recombine to form H_2 which accumulates and produces an increase in pressure and causes the formation of blisters and/or cracks which can lead to fracture of the material [1]. The evaluation and control of corrosion of carbon steel in sour media is very important to the petroleum industry, because this process involved high maintenance costs and equipment replacement. It is also responsible for the loss of human lives and given the importance of corrosion in public safety have established new regulations and practices of corrosion control for pipelines transporting liquids and gases because of the high risk they convey [2,3]. Therefore it is important to know the chemical reactions involved in the different environments of this industry, the type and stability of the corrosion products formed on the surface of the pipe and their effect on the corrosion process allowing a better control of the process reducing risks and costs.

In the literature, several researchers have evaluated the corrosion behavior and film growth by corrosion products in different media simulating different refining conditions, such as media containing $(Cl + H_2S)$, $(NH_4 + Cl + H_2S)$ and $(Cl + CN + H_2S)$. Shoesmith *et al.* [4] and Liu *et al.*, [5] established that the composition of the films of corrosion products depend on the composition of the medium and pH [4,5]. In the process of corrosion of carbon steel in the presence of H_2S , the corrosion product formed is mainly mackinawite [6]. However, it has been noted the formation of an oxide film formed by a combination of mackinawite ($Fe_{(1+x)}S$), troilite (FeS) and iron sulfide amorphous [4,5]. Tewari and Campbell proposed that the steel in H_2S generated solutions Fe_xS_y film. There have been many studies to determine the composition of the corrosion products and their kinetics of formation [7,8]. However, few studies have been conducted on the effect of the flow rate on the composition and morphology of the corrosion products as well as on the corrosion rate on two different micro-alloyed steels. In this work, the study of electrochemical corrosion of new generation pipeline steels is introduced. The corrosion of steel API 5L X-70 NG (new generation) with a carbon content of 0.1 % wt maximum [9] was tested in a brine added with kerosene and 1382.7 ppm of H_2S at 60°C. Linear polarization scans, scanning electron microscopy and X-ray diffraction were applied to determine corrosion rates to be compared with a steel API 5L X-70 T (traditional) with 0.240 wt % of carbon, besides morphology and composition of corrosion products.

2. EXPERIMENTAL PROCEDURE

2.1. Test Environment.

The test solution was a brine prepared according to NACE standard 1D-196 [10] with 106.56 g/L NaCl, 4.48 g/L $CaCl_2 \cdot 2H_2O$, 2.06 g/L $MgCl_2 \cdot 6H_2O$ and 10% kerosene, 1387 ppm of hydrogen sulfide (H_2S) was added. The pH was 3.9 and the temperature of the solution was 60 °C. The test

solution was deaerated with nitrogen gas for a period of 30 minutes as stated in the ASTM G59-97 [11] to remove dissolved oxygen.

2.2. Experimental set up.

A double bottom cell made of Pyrex glass heated with hot water was used. Cylindrical tests specimens were cut off from actual pipes of 11 mm or more of thickness in the longitudinal direction. The total area exposed of the working electrode was 3.5 cm^2 for both static and dynamic tests. The reference electrode was a saturated calomel electrode (SCE), and two auxiliary electrodes of sintered graphite rods were used. Before each experiment, the working electrode was wet abraded to 600 silicon carbide paper, cleaned with deionized water and degreased with acetone. All electrochemical tests were performed on recently clean prepared samples and fresh solutions.

2.3. Hydrodynamic conditions.

The hydrodynamic simulations of flow velocity in the laboratory were carried out in a rotating cylinder electrode (RCE) made by EG & G PARC, model 616 RDE connected to a Potentiostat/Galvanostat. The corrosion rate of the system was evaluated at different electrode rotation rates. The working electrode rotational speeds used in this study were varied from 0 to 6500 rpm (3.74 m/s), with increments of 500 rpm. The selection of these ranges were based on the conditions commonly observed at industrial facilities, as well as on the values of the Reynolds numbers (Re) allowing the validation of the existent hydrodynamic and mass transfer correlations for the RCE. The Reynolds number is from 0 to a value of 17,464.8157 (at 6500 rpm) this being a fully turbulent regime.

2.4 Immersion tests

To carry out immersion tests coupons 1 cm long x 1 cm high were prepared for both steels (API 5L X-70 T and NG), which were immersed for a period of 24 hours in a medium of synthetic brine prepared in agreement to NACE standard ID-196 added with 10% kerosene + 1382.7 ppm H_2S (equivalent to 1 bar pressure) in order to induce corrosion products on both steel surfaces to be analyzed by scanning electron microscopy (SEM) for morphology and distribution.

2.5. Corrosion rate measurements.

For conducting linear polarization resistance measurements the standard for conducting potentiodynamic polarization resistance measurements [11] was applied by means of the commercial software POWER SUIT by using a Potentiostat/Galvanostat of Princeton Applied Research model 263A. The polarization curves were obtained at a scan rate of 0.166 mV/s working in the range of $\pm 200 \text{ mV}$ vs. the open circuit potential (OCP) in reference to SCE. The corrosion rate was obtained as a function of flow rate for the steels tested in the environment. To ensure reliability of results three tests

were taken for each flow velocity range employed, allowing the system to rest for 5 minutes before running the test and recording potential and current density for each of the steels used in the investigation.

2.6. Characterization of corrosion products by SEM.

The surface morphology and composition of the corrosion products formed on the electrode surfaces of traditional and new generation API X-70 steels was analyzed by a JEOL 6300 SEM coupled with EDX.

2.6.1 Physical characterization by XRD

X-ray diffraction (XRD) was used to determine the iron phases on API 5L X-70 (T) and X-70 (NG) steels, with a scanned range from 20° to 90° and a step width of 0.02°, using a D8 Focus Bruker diffractometer with Cu K α radiation. Further analyses of XRD spectra were carried out by the CreaFit 2.2 DRXW software.

3. RESULTS AND DISCUSSION

3.1. Chemical analysis and metallography

The chemical composition of pipe steels was obtained by arc spectrometry (spark) and they are shown below in Table 1.

Table 1. Chemical composition of the API 5L X-70 T and X-70 NG steels (wt. %)

Steel	C	Mn	Si	P	S	Cr	Cu	Ni	Fe
API 5L X-70 (T)	0.240	1.081	0.284	0.019	0.021	0.156	0.185	0.088	97.8
API 5L X-70 (NG)	0.048	0.927	0.222	0.004	0.015	0.017	0.279	0.005	98.4

It can be observed that the API steel 5L X-70 NG has a lower carbon content (0.048 wt%) with respect to the traditional steel (0.240 wt%); it possesses lower amounts of Mn and Si. NG steel also shows an improved cleanliness with lower contents of phosphorus and sulfur. Regarding P has a very low quantity compared to the traditional, which is a typical characteristic of these steels in their manufacturing process. It also has quantities well below the traditional Cr and Ni relative to copper but the new generation has approximately as much as twice Cu compared with the traditional.

3.2 Microstructure and grain size

Figure 1 shows the micrographs carried out on the steels proposed in this research. The images were obtained in the optical microscope, they show the presence of pearlite (dark phase) in a ferrite matrix (white phase). In addition, for the API 5L X-70 NG (b) a slight pearlite banding due to the manufacturing process of this steel is observed, this is in agreement with similar microstructures obtained by others researchers [12-14].

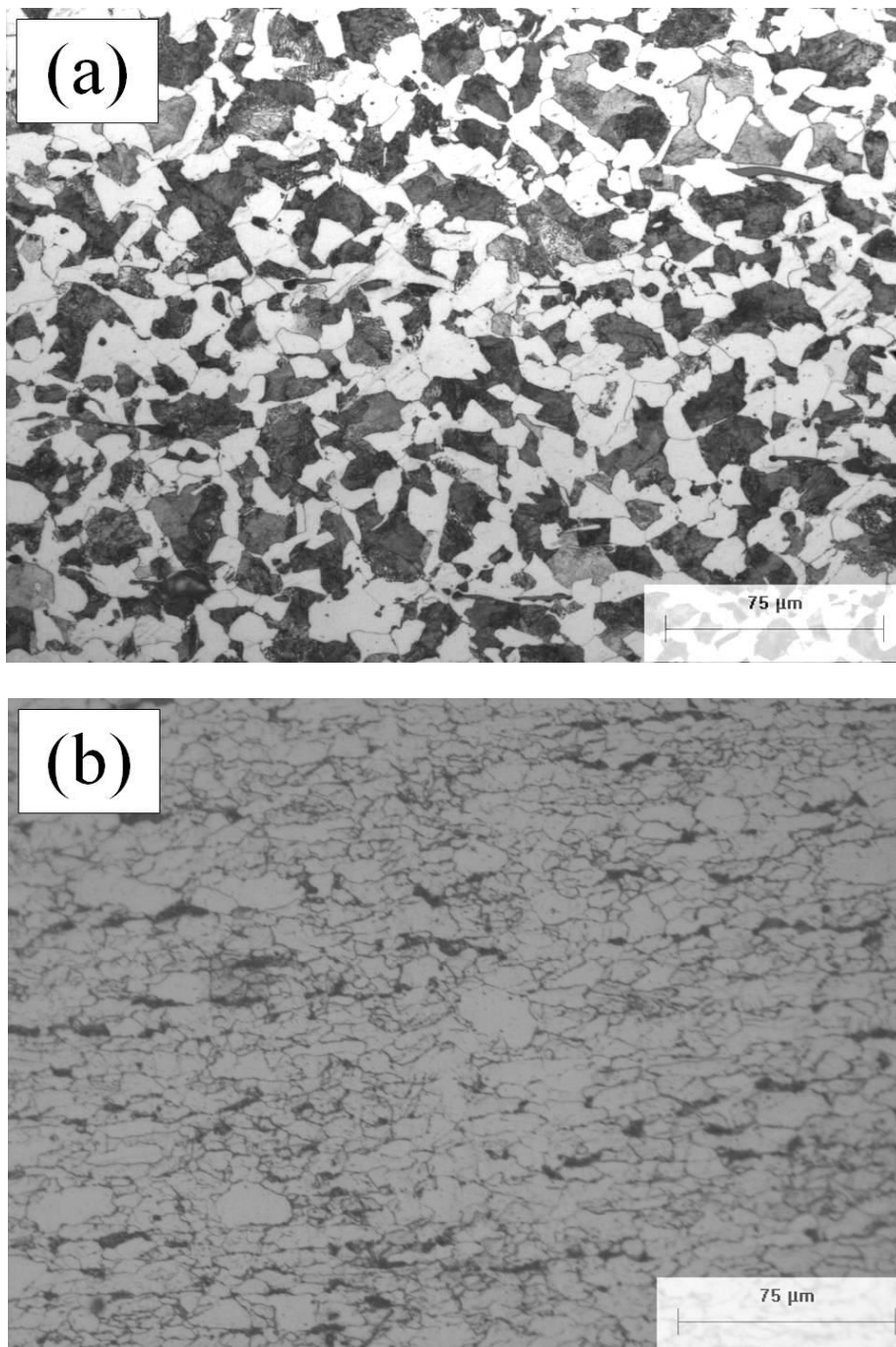


Figure 1. Microstructure of (a) API 5L X-70 T and (b) API 5L X-70 NG steels.

Table 2. Quantitative metallography of API 5L X-70 steels along the longitudinal section.

Steel	% Ferrite	% Pearlite	ASTM Grain
API 5L X-70 T	70.51	29.48	10
API 5L X-70 NG	94.86	5.14	10

Table 2 shows that both steels have the same ASTM grain size with a value of 10, which is a refined grain. With respect to the amount of ferrite of the steel API 5L X-70 NG, it contains more than traditional steel and therefore would be expected that this steel will be more easily dissolved when exposed to the corrosive environment, this effect is not observed on the values of the corrosion rates apparently because of the protective film of copper on NG steel. Likewise, as a result of the lower amount of pearlite, it will not form a larger amount of sulfur compounds as corrosion products, as it is the case of traditional steel, which tend to be deposited on this phase. Pearlite act as cathode by the presence of cementite and thereby to more efficiently protect the steel surface [15].

3.3 Immersion tests

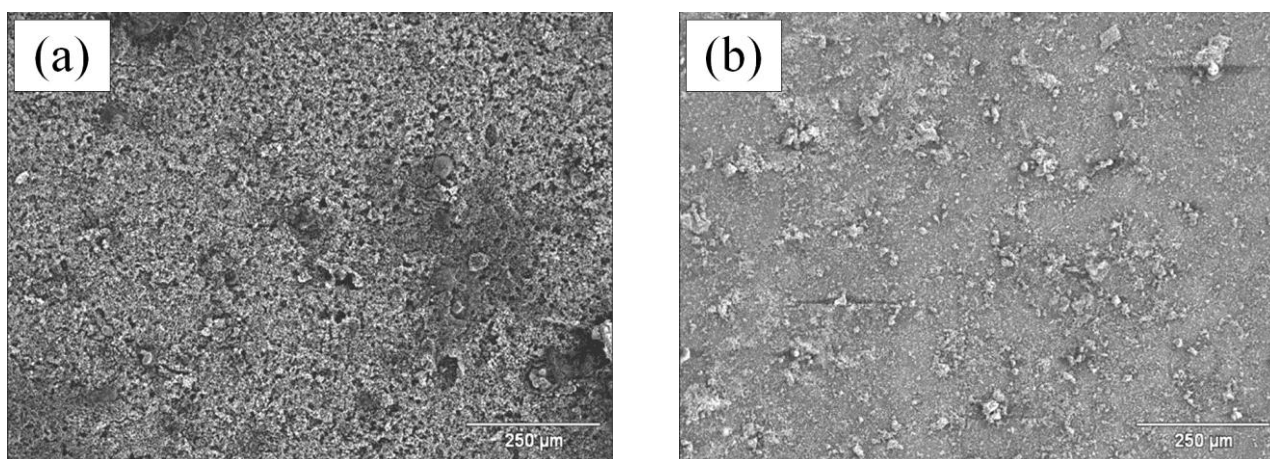
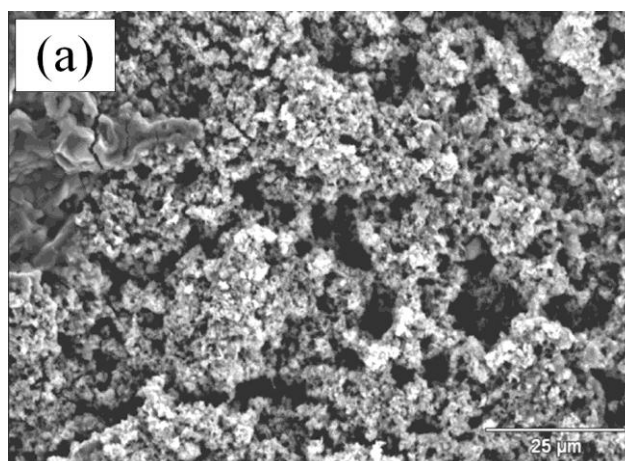


Figure 2. Micrographs of steel API 5L X-70 T (a) and NG (b) at 100X immersion test after 24h.



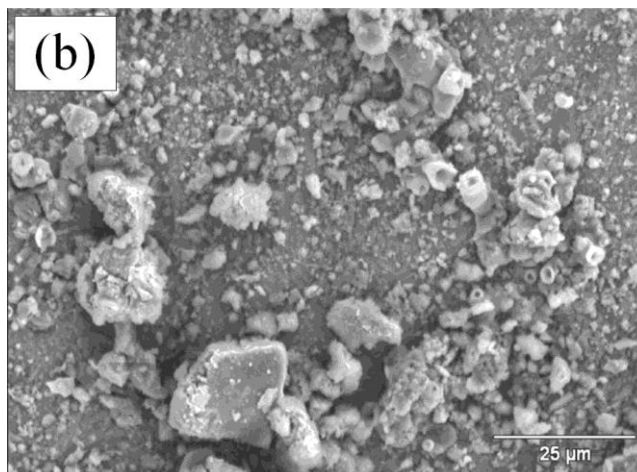


Figure 3. Micrographs of steel API 5L X-70 T (a) and NG (b) at 1000X immersion test after 24h.

Figure 2 shows the uniform corrosion product layer formed on both steels surfaces at 100X, It is observed that steel API 5L X-70 T (a) generated a greater amount of corrosion products than those formed on new generation steel (b), which may have some effect on the corrosion rate.

At higher magnifications (1000X), it can be appreciated the morphology of the corrosion products formed on both steels (Figure 3). The traditional API X-70 displayed a coarser surface with a higher porosity than that deposited on steel API 5L X-70 NG (b). For new generation steel (b) it can be seen that a primarily uniform layer was formed and the corrosion products were deposited in lower amount and the whole surface. As mentioned before nature and morphology may affect the corrosion rate behavior of these steels.

3.4 Linear polarization resistance and corrosion rates

3.4.1 Corrosion potentials for pipe steels as function of flow rates in sour brine at 60 °C.

Figure 4 shows the corrosion potential behavior as a function of the rotation speed with the addition of H₂S at 60 °C. It is observed that both steels started from an active state, one more (API 5L X-70 NG) than the other (API 5L X-70 T), since both have a clean surface free of corrosion products; then the two steels pass into a less active state with a tendency to become independent of the rotational speed, which it may indicate a steady growth of corrosion products. Note that the least active (~ 20 mV) to the end of the test is the API 5L X-70 T. Results show that the corrosion tendency is slightly higher for the API 5L X-70 NG; in this case activity indicated that corrosion products begin to form and evolved uniformly throughout the flow velocity range employed, therefore it is not further seen a significant increase in the tendency to corrosion due to the corrosion potential does not increase greatly, so it could be assumed that the corrosion products formed are more stable and uniform in the NG steel.

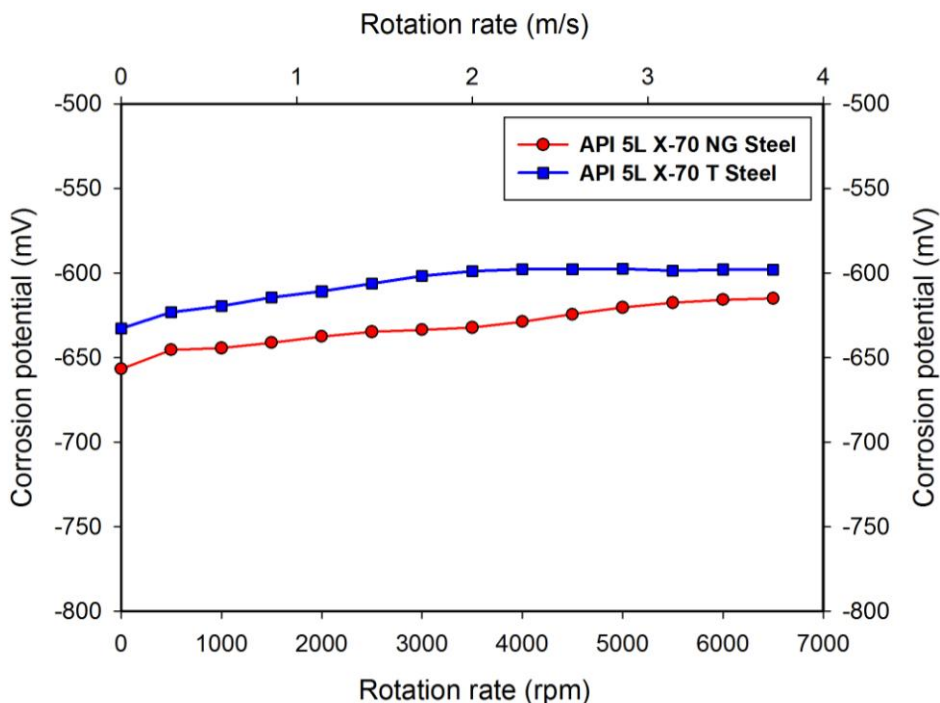


Figure 4. Corrosion potential of API 5L X-70 T and API 5L X-70 NG as a function of flow rate for the steels in sour brine with kerosene added with H₂S at 60 °C.

3.4.2 Comparison of the corrosion rates as function of flow rates for steels API 5L X-70 T and API 5L X-70 NG in sour brine at 60 °C.

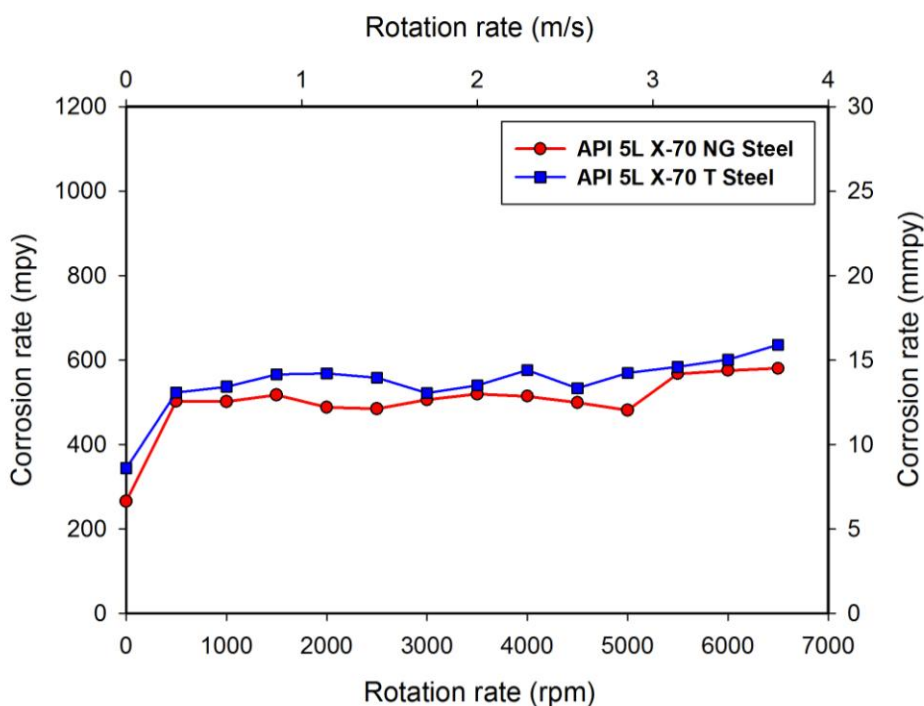


Figure 5. Corrosion rate of API 5L X-70 T and API 5L X-70 NG as a function of flow rate for the steels in sour brine with kerosene added with H₂S at 60 °C.

Figure 5 shows the results for the corrosion rate of pipe steels in sour brine with kerosene and H₂S at 60 °C. From these results, it was observed a high corrosion rate from the very beginning for API 5L X-70 T (8 mm/y) and API 5L X-70 NG (9 mm/y), later corrosion rate increased with the increase in the flow rate to reach a top of about 15 mm/y. The variation of the corrosion rate with the flow velocity is generally attributed to changes in the corrosion mechanism [16]. These steels showed a similar behavior, which suggests that the corrosion products formed on surface are more stable as there is not significant detachment of the corrosion products. The API 5L X-70 T tested between 6000 and 6500 rpm shows an increase in the corrosion rate, which indicated that there was a detachment of the corrosion products formed as a result of fluid turbulence and consequently the wall shear stresses diminished the thickness of this layer [17], which led to an increase of the corrosion rate, so this steel (T) may not be quite stable or have a good adherence when compared to the NG steel. In the case of API 5L X-70 NG, it was observed that within 5500 to 6500 rpm, the corrosion rate remains almost constant due to the continuous formation of corrosion products on steel, besides its corrosion rate is slightly lower compared to API 5L X-70 T.

API 5L X-70 NG displayed a higher corrosion resistance than API 5L X-70 T. In this case the microstructure apparently had no effect on the corrosion rate. The latter steel would expect to have a better behavior than that of API 5L X-70 NG, because it has a greater amount of perlite (34.2%) compared to the ferrite (65.89%), as ferrite is more easily dissolved in the aggressive environment. In contrast, API 5L X-70 NG possesses 6.10% pearlite and 93.90% ferrite so that it was expected to display an increase in corrosion rate by the increased presence of this phase [18], which can be dissolved in a larger volume but not homogeneously. Additionally both steels have the same grain size so it is assumed that this parameter has no effect on the corrosion rate.

The steel API 5L X-70 T has a greater amount of phosphorus (0.019 wt%), chromium (0.156 wt%) and nickel (0.088 wt%) with respect to X-70 NG, which contains 0.009 wt% of phosphorus, chromium (0.013 wt%) and nickel (0.005 wt%), but it contains more copper than the traditional (T) with a 0.286 wt%, which is almost twice of X-70 T, so it appears that Cu in X-70 NG is the responsible of the improvement in corrosion resistance as a result of the formation of high stability oxides. As chromium and nickel has the quality to be combined with sulfur to reduce the damaging effect on the traditional API X-70 (T) and some authors assumed that cathodic reaction in presence of oxygen contributed to film formation, therefore corrosion resistance of traditional X-70 is derived from the synergetic effect of chromium and nickel to form an insoluble rust layer at the initial stage of corrosion as suggested by Choi *et al.* [19].

3.5 SEM surface characterization

Figure 6 display SEM micrographs from steel surfaces at low magnification (100X). It is observed that corrosion products have certain similarities; the presence of a uniform layer that is evident and which eventually overgrows the corrosion products. In micrograph (b) a greater degree of cracking can be appreciated but not any kind of detachment, feature associated with a dramatic increase in the corrosion rate as discussed in Figure 6.

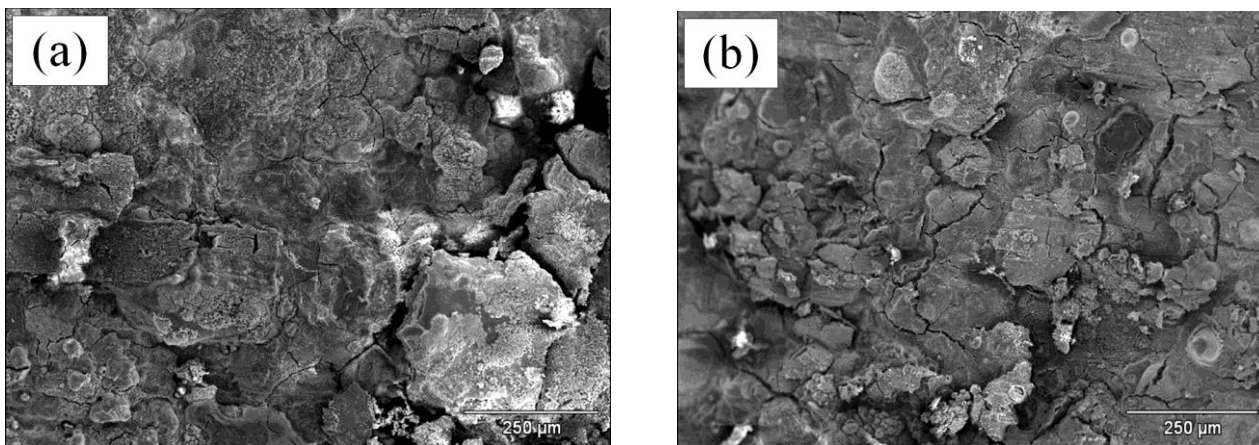


Figure 6. Micrographs of steel API 5L X-70 T (a) and API 5L X-70 NG (b) at 100X.

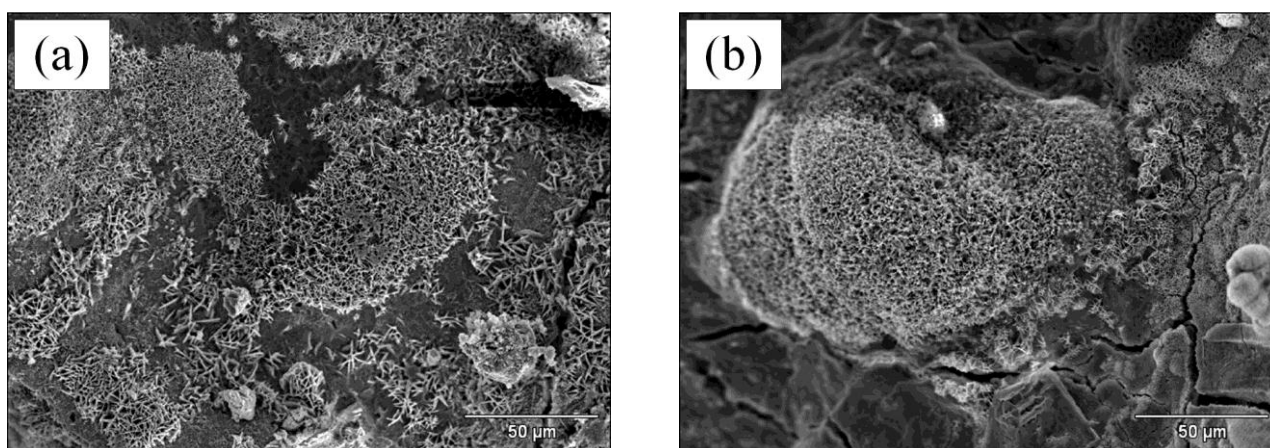


Figure 7. Micrographs of steel API 5L X-70 T (a) and API 5L X-70 NG (b) at 500X.

In Figure 7 the two steel surfaces at higher magnification (500X) are shown, It is observed in more detail that the corrosion products grown on a first layer, which have the form cactus type; fact that has already been reported by some authors [20]. Corrosion products seem to be quite porous and to some point brittle as seen in micrograph (b), where NG steel shows cracks, which appears to be the result of the material detached because of fluid flow action, thus there may be areas where the metal is not protected to a certain degree so that corrosion is active.

Figure 8 and 9 show the mapping images of steels API 5L X-70 T and API 5L X-70 NG after corrosion tests, where O, S and Fe are identified. These elements indicate the presence of a protective layer of FeO, Fe₂O₃, Fe₃O₄, besides some sulfides such as mackinawite (FeS_{1-x}) on the film formed and corrosion products, as reported in the literature [21-23]. Figure 8 also shows that carbon, iron, chromium and nickel are distributed all over the analyzed surface, while oxygen and sulfur are displayed in certain regions in a higher proportion than that of the general distribution. This is an indication that there exist regions where a greater amount of oxides and sulfides predominated as is the case for the X-70 NG.

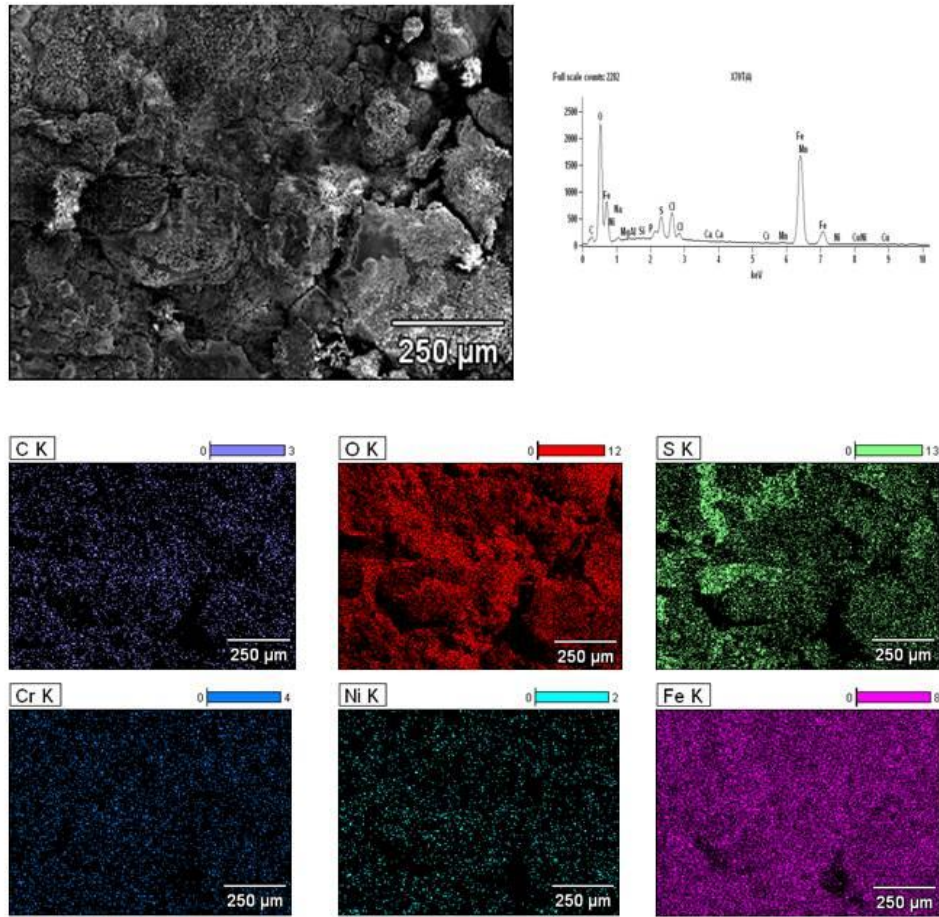


Figure 8. EDX-SEM microanalyses by element after corrosion tests in sour brine for API 5L X-70 T.

Table 3. Chemical composition (wt %) of corrosion scale on API 5L X-70 T.

Element Line	Weight %	Atom %
C K	11.36	24.53
O K	27.81	45.09
Na K	0.92	1.04
Si K	0.03	0.03
S K	1.89	1.53
Cl K	3.07	2.25
Ca K	0.01	0.00
Cr K	0.17	0.09
Mn K	0.58	0.27
Ni K	0.23	0.10
Cu K	0.00	0.00
Fe K	53.94	25.06
Total	100.00	100.00

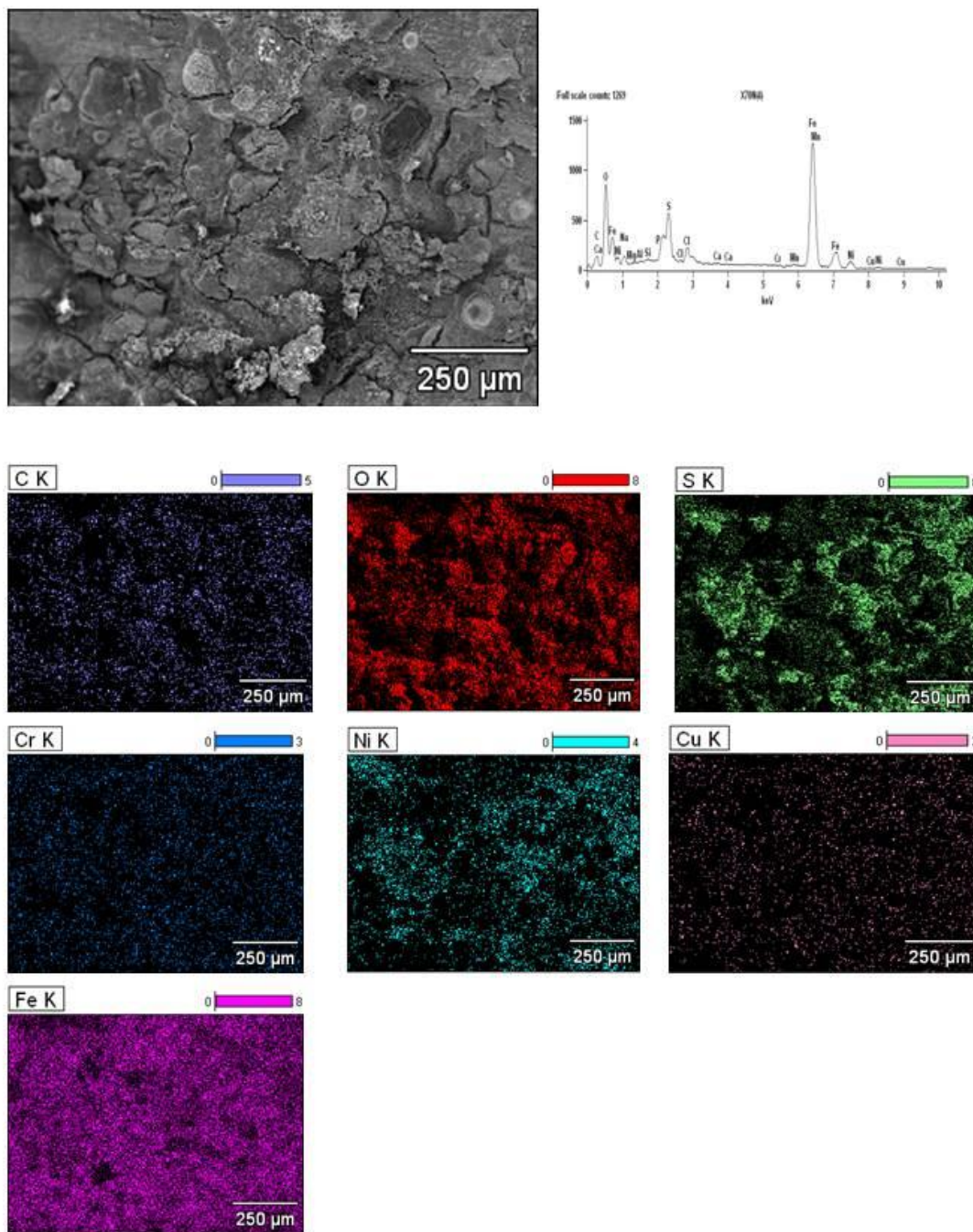


Figure 9. EDX-SEM microanalyses by element after corrosion tests in sour brine for API 5L X-70 NG.

Table 3 shows the results obtained by EDX microanalysis for API 5L X-70 T, where the elements with greater presence are (wt %): C-11.36, Fe-93.94, O-27.81 and S-1.89, which suggests that the combination of these elements generated a larger content of both sulfides and oxides than those contained in steel X-70 NG (Table 4). Chromium (0.17 wt%) and nickel (0.23 wt%) present indicates that these elements in combination with oxygen could form the corresponding oxides and sulfides, which are highly stable and contribute to corrosion control.

Table 4. Chemical composition (wt %) of corrosion scale on API 5L X-70 NG.

Element Line	Weight %	Atom %
C K	13.95	33.09
O K	16.31	29.05
Na K	1.61	1.99
Si K	0.21	0.21
S K	2.83	2.51
Cl K	0.14	0.11
Ca K	0.16	0.11
Cr K	0.13	0.07
Mn K	0.37	0.19
Ni K	5.43	2.64
Cu K	0.29	0.13
Fe K	58.58	29.89
Total	100.00	100.00

Figure 9 shows the presence of carbon, iron, chromium, nickel and copper distributed all over the analyzed surface of X-70 NG. Oxygen, sulfur and nickel are distributed on the entire surface though there are areas with a higher content of these elements. It is observed that oxygen, sulfur, nickel, chromium and copper seems to be present in a higher proportion than in X-70 T, which is not true as seen in Tables 3 and 4. It is thought then that the distribution of these elements on steel X-70 NG surface formed more stable compounds forming a tougher film for corrosion control and consequently seems to appear in a higher concentration on surface when compared to X-70 T.

3.6 XRD Characterization of corrosion products

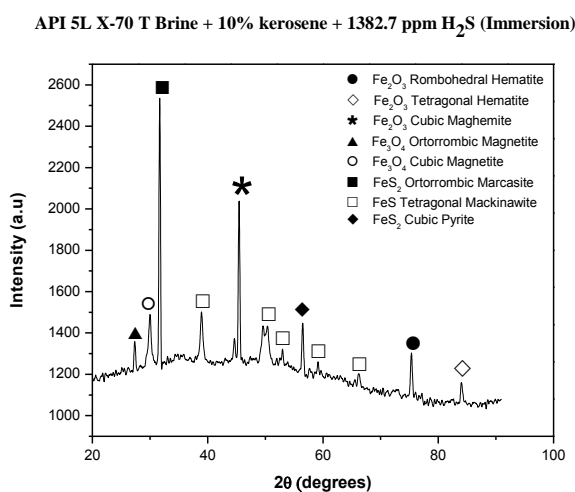


Figure 10. XRD analysis of corrosion products in API 5L X-70 T after immersion test for 24 hours in sour brine.

Figure 10 shows the diffraction pattern obtained for the steel API 5L X-70 T after 24 h of immersion in the corrosive environment. Steel surface displayed a wide variety of corrosion products to conform a mixture of oxides and sulfides. Crystalline structures with distinct phase were identified, such as the most predominant orthorhombic Marcasite (FeS_2), cubic maghemite (Fe_2O_3) and tetragonal mackinawite (FeS). It is also observed that sulfides formed over oxides, which causes an improved behavior on corrosion resistance.

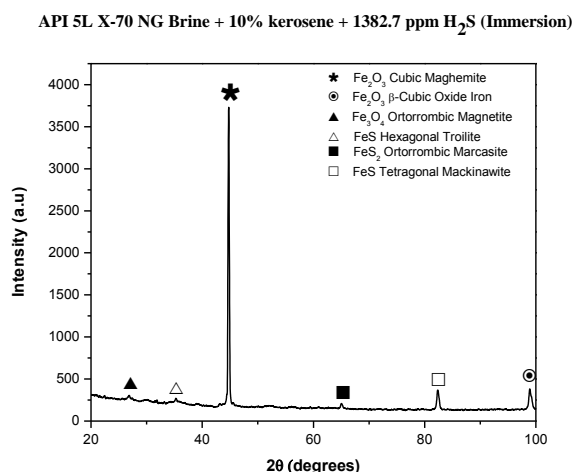


Figure 11. XRD analysis of corrosion products in API 5L X-70 NG after immersion test for 24 hours in sour brine.

For steel API 5L X-70 NG, the formation of corrosion products on the surface after carrying out the immersion test for 24 hours is observed in Figure 11. X-70 NG provided a much smaller range of phases, where predominates oxides on the formation of sulfides. In this case, the phase formed in the largest amount was identified as cubic maghemite (Fe_2O_3). It is important to mention that this phase is protective but to some extent as it has been reported that an oxide is less protective than a sulfide [24].

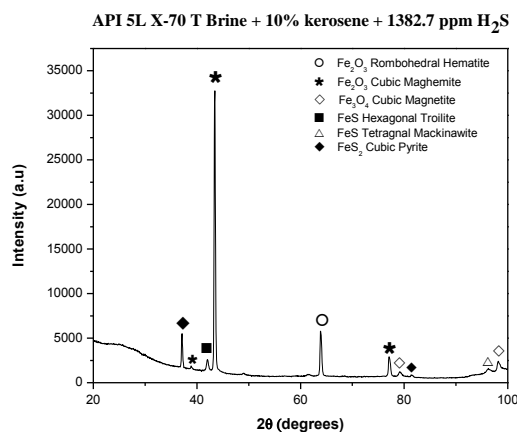


Figure 12. XRD analysis of corrosion products deposited on API 5L X-70 T steel surface after corrosion tests in a sour brine solution.

In Figure 12, a diffraction pattern obtained for the steel API 5L X-70 T in the corrosive medium used is observed. In this case it is possible to see that a mixture of oxides with sulfides are formed with different crystal structures to be the predominant phase that identified as cubic maghemite (Fe_2O_3), which also appears in the immersion test.

The two steels formed oxides such as hematite (rhombohedral), maghemite (cubic) and magnetite (cubic), and also sulphides such as mackinawite (tetragonal), troilite (hexagonal) and pyrite (cubic and triclinic). Mackinawite is a common mineral composed of tetragonal crystals, whereas troilite is hexagonal though both are considered protective layers. The different crystal structures of iron sulfides formed in H_2S containing corrosive media were described in detail by D. Rickard *et al.* [25]. The crystal structures of the corrosion products in film significantly vary from each other [26], whereas the differences in the crystal structures of iron sulfide are derived from differences in the corrosive medium [27].

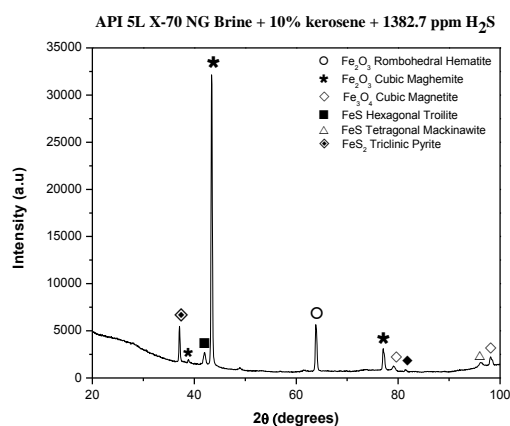


Figure 13. XRD analysis of corrosion products deposited on API 5L X-70 NG steel surfaces after corrosion tests in a sour brine solution.

The presence of some oxides like Fe_2O_3 and Fe_3O_4 [24] partially protects the steel surface from further dissolutions. It is also noted that oxides predominated much more (peak intensity) than sulfides, even so there was a better protection for X-70 NG steel, which slightly reduced corrosion rate in comparison to X-70 T (~4 mm/y). It is further note that the two steels form sulfides, which are considered protective due to its stability and their crystalline structure as it is the case of hexagonal troilite, tetragonal mackinawite and pyrite phase. However, for steel X-70 NG where a better protective behavior was found triclinic pyrite was present (Figure 13), this phase is more compact compared to cubic pyrite that was formed on steel surface of X-70 T.

4. CONCLUSIONS

Although both steels have different microstructures, X-70 NG has more ferrite to be dissolved, however this parameter seems no to be a factor that influences corrosion resistance.

The improved performance of X-70 NG may be attributed to a synergistic work of Cr, Cu; Ni and P. In the case of new generation steel, copper is in approximately twice as much compared to the traditional steel, this can be combined with decreasing sulfur and their harmful effect and additionally favors the cathodic reaction where oxygen is formed. Chromium and nickel helps retard only anode reaction (dissolution of the ferrite).

The presence of copper in the corrosion products is essential for corrosion resistance, as it is considered that works like chromium and nickel to form highly stable oxides on the steel surface, and also Cu allowed forming a mixture of oxides and sulfides.

The diversity of corrosion products identified on the surface of each steel is very important since they together have a protective function, even though the quantitative analysis shows that a greater amount of oxides (X-70 NG) are formed respect to sulfides (X-70 T), these latter compounds improved corrosion behavior and are more stable than the oxides and may become dissolved by the same action of the corrosive medium.

ACKNOWLEDGEMENTS

The authors would like to thank the Consejo Nacional de Ciencia y Tecnología-México (CONACYT) for sponsorship. Acknowledgments are also due to the Instituto Politécnico Nacional (IPN), Instituto Mexicano del Petróleo (IMP) and the Group of Pipe Integrity Analysis (GAID) for the facilities provided and financial aid, respectively.

References

1. T.A. Ramanarayanan, S.N. Smith, *Corros.*, 46 (1) (1990) 66.
2. B.G. Pound, R.M. Sharp, G.A. Wright, *Aust. J. Chem.* 38 (1985) 1133-1140.
3. P.H. Tewari, M.G. Bailey, A.B. Campbell, *Corros. Sci.*, 19 (7) (1979) 573-585.
4. D.W. Shoesmith, P.M. Taylor, G. Bailey, D.G.J. Owen, *Electrochem. Soc.*, 127 (1980) 1007.
5. C. Liu, Q. Bi, A. Leyland, A. Matthews, *Corros. Sci.*, 45 (6) (2003) 1243-1256.
6. A.G. Wikjord, T.E. Rummery, F.E. Doern, D.G. Owen, *Corros. Sci.*, 20 (5) (1980) 651-671.
7. R. Cabrera-Sierra, I. González, E. Sosa, T. Oropeza, *Electrochim. Acta*, 47 (2002a) 2149.
8. A. Hernández Espejel, A. Ramírez López, P. Vite Martínez, L. Demedices García, *Avances en Ciencias e Ingeniería*, 1, (2010) 45-47.
9. F.F. Eliyan, E. Mahdi, A. Alfantazi, *Corros. Sci.*, 58 (2012) 181-191.
10. NACE 1D-196: "Laboratory Test Methods for Evaluating Oilfield Corrosion Inhibitors" (Houston TX:NACE, 1996).
11. ASTM G59-97 (Reapproved 2003). "Standard Test Method for Conducting Potentiodynamic Polarization Resistance Measurements" (Houston TX:NACE, 2003).
12. R. Dong, I. Sun, Z. Liu, X. Wang and Q. Liu, *Journal of Iron and Steel Research International*, 15 (2008) 71.
13. D. Clover, B. Kinsella, B. Pejicic and R. De Marco, *Journal of Applied Electrochemistry*, 35 (2005) 139.
14. C.W. Du, X.G. Li, P. Liang, Z.Y. Liu, G.F. Jia and Y.F. Cheng, *Journal of Materials Engineering and Performance*, 18 (2009) 216.
15. J.L. Mora-Mendoza, S. Turgoose, *Corros. Sci.*, 44, (2002) 1223-1246.
16. U. Lotz, *Corrosion/90*, Paper no. 27 (Houston TX:NACE International, 1990).
17. D. Silverman, *Corrosion/90*, Paper no. 13 (Houston TX:NACE International, 1990).

18. R. Quiroz, A. Rosales, E. Barón, *Rev. LatinAm. Metal. Mater*; 29 (2), (2009) 84-92.
19. Y.S. Choi, J.J. Shim, J.G. Kim, *Journal. of Alloys and Compounds*, 391 (2005) 162.
20. S. Seal, K. Sapre, A. Kale, V. Desai, M. Gopal, P. Jepson, *Corr. Sci.*, 42 (2000) 1623-1634.
21. R. N. Tuttle, R. D. Kane, *A Compilation of Classic Papers*, NACE, Houston, Texas (1981).
22. F. H. Meyer, O. L. Riggs, R. L. McGlasson, J. D. Sudbury, *Corrosion*, 14 (1958) 69.
23. S. N. Smith, E. J. Wright, *Corrosion/94*, Paper no. 011 (Houston, TX: NACE International, 1994).
24. El-Sayed M. Sherif, Abdulhakim A. Almajid, Khalil Abdelrazek Khalil, Harri Junaedi and F.H. Latief, *Int. J. Electrochem. Sci.*, 8 (2013) 9360.
25. D. Rickard and G. Luther, *Chem. Rev.*, 107 (2007) 514.
26. D. Rickard, J. Morse, *Mar. Chem.*, 97 (2005) 141.
27. E. Díaz, J. Gonzalez-Rodriguez, R. Sandoval-Jabalera, S. Serna, B. Campillo, M.A. Neri-Flores, C. Gaona-Tiburcio, A. Martínez-Villafañe, *Int. J. Electrochem. Sci.*, 5 (2010) 1821.

© 2015 The Authors. Published by ESG (www.electrochemsci.org). This article is an open access article distributed under the terms and conditions of the Creative Commons Attribution license (<http://creativecommons.org/licenses/by/4.0/>).